1 **Decoupling the impact of microRNAs on translational repression versus RNA**

2 **degradation in embryonic stem cells**

3

4 **Jacob W. Freimer 1, TJ Hu 1, and Robert Blelloch 1***

5

6 **1 The Eli and Edythe Broad Center of Regeneration Medicine and Stem Cell Research,**

7 **Center for Reproductive Sciences, University of California, San Francisco, 35 Medical**

8 **Center Way, San Francisco, CA 94143, USA; Department of Urology, University of**

9 **California, San Francisco, 35 Medical Center Way, San Francisco, CA 94143, USA.**

10

11 ***Correspondence: robert.blelloch@ucsf.edu.**

12

13 **ABSTRACT**

14 Translation and mRNA degradation are intimately connected, yet the mechanisms that regulate

15 them are not fully understood. Here we studied the link between translation and mRNA stability

16 in embryonic stem cells (ESCs). Transcripts showed a wide range of stabilities, which correlated

17 with their translation levels. The protein DHH1 links translation to mRNA stability in yeast;

18 however loss of the mammalian homolog, DDX6, in ESCs did not disrupt the correlation across

19 transcripts. Instead, the loss of DDX6 led to upregulated translation of microRNA targets,

20 without concurrent changes in mRNA stability. The *Ddx6* knockout cells were phenotypically

21 and molecularly similar to cells lacking all microRNAs (*Dgcr8* knockout ESCs). These data show

22 that the loss of DDX6 can separate the two canonical functions of microRNAs: translational

23 repression and transcript destabilization. Furthermore, these data uncover a central role for

24 translational repression independent of transcript destabilization in defining the downstream

25 consequences of microRNA loss.

26

27 **INTRODUCTION**

28 Gene expression is determined through a combination of transcriptional and post-transcriptional

29 regulation. While transcriptional regulation has been extensively studied, less is known about

30 how the regulation of mRNA stability contributes to overall mRNA levels. Mammalian mRNAs

31 display a wide range of half-lives ranging from minutes to over a day (Schwanhäusser et al.,

32 2011). The wide range of mRNA stabilities are regulated by both intrinsic sequence features as

33 well as the binding of regulatory factors such as microRNAs and RNA-binding proteins (Cheng,

34 Maier, Avsec, Rus, & Gagneur, 2016; Hasan, Cotobal, Duncan, & Mata, 2014; Wu & Brewer,

35 2012). However, the identity of such features and regulatory factors as well as how they impact

36 mRNA stability are not well understood.

37

38 One process that is intimately linked to mRNA decay is translational repression (Roy &

39 Jacobson, 2013). Quality control mechanisms such as nonsense mediated decay, no go decay,

40 and non stop decay sense aberrant translation and lead to mRNA degradation (Parker, 2012;

41 Shoemaker & Green, 2012). Translational repression and mRNA decay are also linked

42 independent of either a quality control or a stress response (Huch & Nissan, 2014). In yeast,

43 inhibition of translation initiation through either 5' cap binding mutants or drug treatment leads to

44 accelerated mRNA decay (Chan, Mugler, Heinrich, Vallotton, & Weis, 2017; Huch & Nissan,

45 2014; Schwartz & Parker, 1999). Conversely treatment with cycloheximide, which blocks

46 ribosome elongation, stabilizes mRNAs (Beelman & Parker, 1994; Chan et al., 2017; Huch &

47 Nissan, 2014). How upstream factors influence mRNA stability through the regulation of

48 translation initiation and elongation is poorly understood.

49

50 Whether microRNAs (miRNAs) primarily impact translation or mRNA degradation has been

51 intensely debated (Iwakawa & Tomari, 2015; Jonas & Izaurralde, 2015). MiRNAs are small,

52 non-coding RNAs that bind to the 3' UTR of their target transcripts to inhibit translation and/or

53 induce mRNA destabilization (Fabian & Sonenberg, 2012; Jonas & Izaurralde, 2015). The

54 impact of miRNAs on the translation and expression of endogenous transcripts has been

55 measured using ribosome profiling which measures the ratio of ribosome protected fragments to

56 input mRNA (this ratio is termed translational efficiency) and RNA-Seq which measures RNA

57 levels. Simultaneous ribosome profiling and RNA-Seq experiments across a number of contexts

58 show that miRNAs produce larger changes in mRNA levels than in translation efficiency, leading

59 the authors to suggest that mRNA destabilization is the dominant effect of miRNA repression

60 (Eichhorn et al., 2014a; Guo, Ingolia, Weissman, & Bartel, 2010a). However, in other studies, it

61 has been suggested that miRNAs primarily inhibit translation levels. For example, in the early

62 zebrafish embryo, ribosome profiling and RNA-Seq show that miRNAs induce translational

63 repression without mRNA destabilization (Bazzini, Lee, & Giraldez, 2012). Furthermore,

64 experiments using miRNA reporters to examine the kinetics of miRNA repression suggest that

65 translational repression precedes mRNA destabilization (Béthune, Artus-Revel, & Filipowicz,

66 2012; Djuranovic, Nahvi, & Green, 2012). These studies raise the question of whether

67 translational repression is the direct mode of miRNA-driven suppression and whether mRNA

68 destabilization is a secondary consequence. To resolve this question, it is important to

69 genetically separate the two functions. However, despite extensive research, it is not known

70 whether it is possible to decouple miRNA-induced translational repression and mRNA

71 destabilization of endogenous transcripts in a cell where both occur.

72

73 The RNA-binding protein DDX6 and its yeast homolog DHH1 are DEAD box helicases that

74 localize to P-bodies and stress granules and have been implicated in both translational

75 repression and mRNA destabilization, suggesting that they may link these two processes (Coller

76 & Parker, 2005; Vlad Presnyak & Coller, 2013). Tethering experiments in yeast that lack DCP2

77 or DCP1 demonstrate that DHH1 can repress translation upstream and independent of

78 enhancing decapping (Carroll, Munchel, & Weis, 2011; Sweet, Kovalak, & Coller, 2012).

79   Tethering experiments in human cells demonstrate that DDX6 also represses translation

80   (Kuzuoğlu-Öztürk et al., 2016a). Furthermore, DDX6 binds to components of the decapping

81   complex, but exactly how this impacts translation and mRNA stability is unclear (Ayache et al.,

82   2015; Nissan, Rajyaguru, She, Song, & Parker, 2010; Tritschler et al., 2009). Additionally,

83   through interactions with the CCR4-NOT complex and the decapping complex, DDX6 is thought

84   to be involved in miRNA mediated translational repression, but its exact role is not fully

85   understood (Y. Chen et al., 2014a; Chu & Rana, 2006; Mathys et al., 2014a; Rouya et al.,

86   2014a).

87

88   Here we sought to understand how mRNA stability changes are linked to translation changes

89   during early mammalian development. It has been suggested that up to 70% of the molecular

90   changes during mouse embryonic stem cell (ESC) differentiation are due to post-transcriptional

91   regulation (Lu et al., 2009a). Therefore, we measured and analyzed changes in mRNA stability

92   and translation efficiency during ESC differentiation. Surprisingly, we found that the vast

93   majority of molecular changes during this transition are driven by transcriptional, not post-

94   transcriptional mechanisms. However, within self-renewing ESCs there was a wide range of

95   mRNA stabilities. These stability differences correlated with translational levels. We generated

96   *Ddx6* KO ESCs to determine whether DDX6 links translation to stability. Unlike its yeast

97   homolog, DDX6 did not appear to play a general role in linking the two. However, its loss did

98   lead to the translational upregulation of miRNA targets with little associated changes in mRNA

99   stability. The resulting cells looked phenotypically and molecularly similar to cells deficient for all

100   miRNAs. Therefore, the loss of DDX6 is able to separate the two central functions of miRNAs:

101   translational repression and mRNA destabilization. Furthermore, these data show miRNA

102   induced translational repression alone can recapitulate many of the downstream consequences

103   of miRNAs.

104

105 **RESULTS**

106 **Transcriptional changes drive expression changes during the ESC to EpiLC transition**

107 Previous work suggested that up to 70% of the molecular changes that occur during early ESC

108 differentiation are due to post-transcriptional events (Lu et al., 2009b). In that work,

109 differentiation was induced by expressing a shRNA to Nanog in ESCs grown in LIF. These

110 conditions are associated with a heterogeneous population of cells (Ivanova et al., 2006). To

111 revisit this question, we first turned to a reporter system and an optimized differentiation protocol

112 that enables the homogenous differentiation of naive ESCs to formative epiblast like cells

113 (EpiLC), which is representative of the transition from the pre- to post-implantation epiblast in

114 vivo (A. Chen et al., n.d.; Krishnakumar et al., 2016; Parchem et al., 2014) (Figure 1A). Using

115 this system, we characterized the changes in mRNA expression, mRNA stability, and translation

116 that occur during the transition. RNA-Seq showed 1890 genes significantly up-regulated and

117 1532 genes significantly down-regulated during the ESC to EpiLC transition (Figure 1B, 1F).

118 Known naive markers were down-regulated, while known primed markers were up-regulated

119 during this transition (Figure 1 - figure supplement 1A) (Boroviak et al., 2015).

120

121 In order to directly measure changes in transcription during the ESC to EpiLC transition, we

122 used metabolic labeling with 4-thiouridine (4sU) (Dolken et al., 2008; Rabani et al., 2011;

123 Windhager et al., 2012). Nascent transcripts were labeled with a thirty-minute 4sU pulse,

124 biotinylated, pulled down with streptavidin, and sequenced (4sU-Seq). Total RNA-Seq was

125 performed in parallel and the ratio of nascent RNA to total RNA was used to calculate relative

126 stabilities for each gene (Rabani et al., 2011). To validate these findings, a subset of genes

127 spanning a range of stabilities were measured using an alternative method where transcription

128 was blocked with actinomycin D and mRNA levels followed over a time course by RT-qPCR

129 (Figure 1 - figure supplement 1B, 1C). The relative stabilities predicted by the two approaches

130 were highly correlated. Given that the 4sU-Seq approach avoids the secondary effects
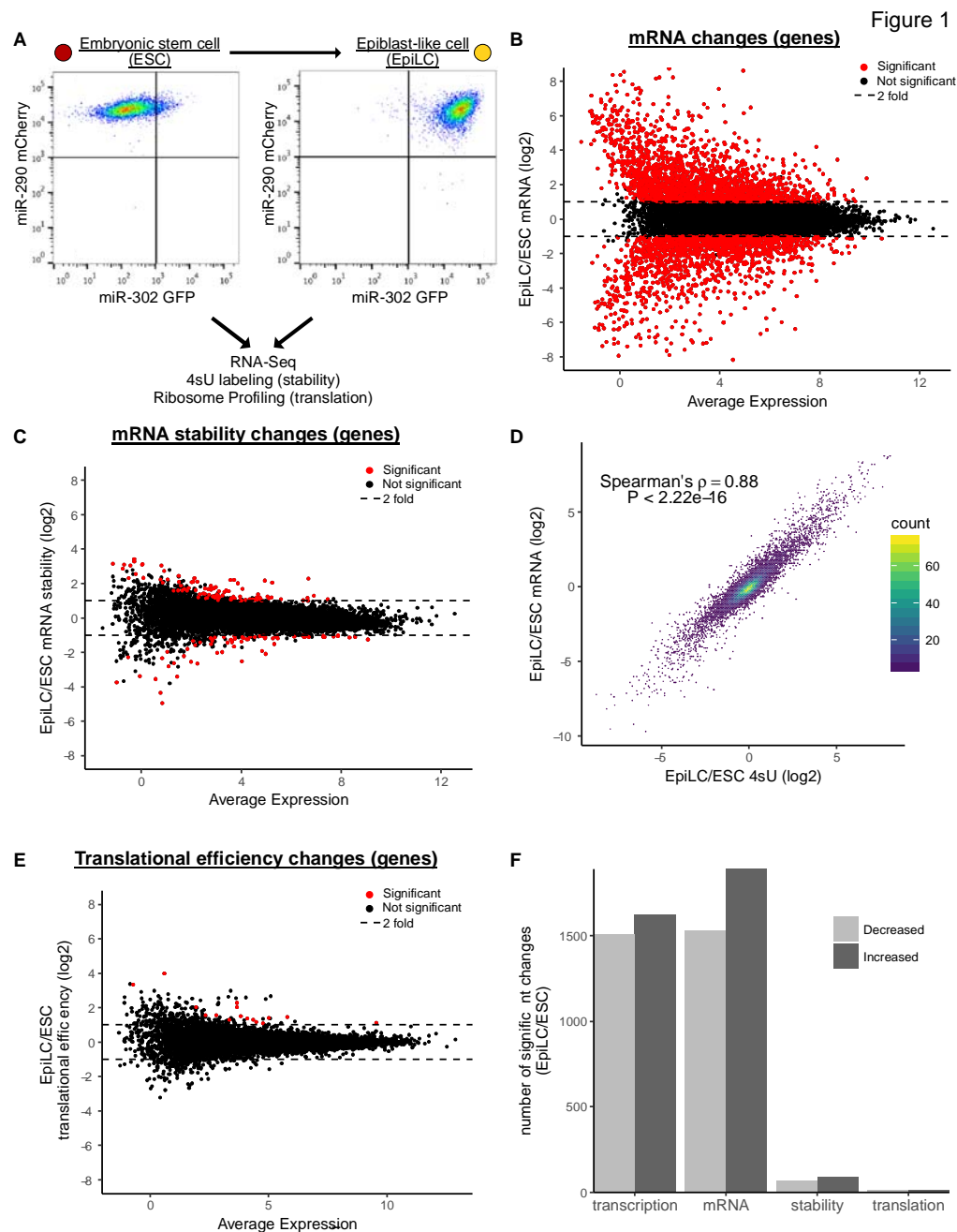
131

Figure 1 Transcriptional changes drive expression changes during the ESC to EpiLC transition.
A) Flow cytometry of the transition from naïve embryonic stem cells (ESCs) (miR-302 GFP-, miR-290 mCherry+) to primed epiblast-like cells (EpiLCs) (miR-302 GFP+, miR-290 mCherry+). B) MA plot of mRNA changes during the ESC to EpiLC transition. Significant changes are shown as red dots (Adjusted P Value < 0.05 and |log2 fold change| > 1) in B, C, E. Dashed lines indicated a 2 fold change. C) MA plot of mRNA stability changes during the ESC to EpiLC transition. D) Correlation between changes in nascent transcription (4sU labeled mRNA) and changes in mRNA levels during the ESC to EpiLC transition. P value calculated with correlation significance test. E) MA plot of translational efficiency (TE) changes during the ESC to EpiLC transition. F) The number of significant increases or decreases in transcription, mRNA levels, mRNA stability, and translational efficiency during the ESC to EpiLC transition. N = 3 for each ESC and EpiLC seq experiment. See also figure 1 - figure supplement 1.

6

143   associated with blocking all transcription, we used those data for genome-wide analysis

144   (Bensaude, 2011; Lugowski, Nicholson, & Rissland, 2017). Surprisingly, the 4sU/total mRNA

145   data showed very few changes in mRNA stability between the ESC and EpiLC states (Figures

146   1C, 1F). This lack of changes was not because of noise among the replicates, as biological

147   replicates were well correlated (Figure 1 - figure supplement 1D).

148

149   The general lack of changes in mRNA stability suggested that transcription is the dominant

150   regulator of the mRNA changes during the ESC to EpiLC transition. Indeed, fold changes in

151   total mRNA levels correlated extremely well with fold changes in 4sU labeled nascent

152   transcripts (Spearman's rho 0.88; $P < 2.22*10^{-16}$) (Figure 1D). Thus, nascent transcription,

153   not mRNA stability, underlies the mRNA changes associated with the ESC to EpiLC transition.

154

155   Next, we asked whether changes in translational levels play an important role in the ESC to

156   EpiLC transition. To measure translational levels of all genes, we performed ribosome profiling

157   to collect Ribosome Protected Footprints (RPFs) and matched total mRNA (Ingolia, Lareau, &

158   Weissman, 2011). As expected, RPFs showed a strong 3 nucleotide phasing of reads that was

159   not present in the mRNA samples, confirming the quality of the data (Figure 1 - figure

160   supplement 1E). We calculated translation using the ratio of RPF/mRNA, also known as

161   translational efficiency (Ingolia et al., 2011). Global analysis showed very few changes in

162   translational efficiencies between the ESC and EpiLC states (Figures 1E, 1F). Biological

163   replicates were well correlated showing that the overall lack of changes is not due to noise

164   between the replicates (Figure 1 - figure supplement 1F). Therefore, like mRNA stability, there

165   are few changes in translation levels, independent of mRNA levels, in early ESC differentiation.

166

167   **There is a wide range of RNA stabilities which are positively correlated with translation**

168   **level in ESCs.**

7

169   Although there were minimal changes in mRNA stability during the ESC to EpiLC transition,

170   there was a wide range of mRNA stabilities within ESCs. For example, between the 25th and

171   75th percentile of mRNA stability, there was a 3.2 fold difference in stability and between the top

172   and bottom 1% of mRNA stability there was over a 64 fold difference (Figure 2A). To identify

173   features that explain the range of mRNA stabilities observed, we performed multiple linear

174   regression taking into account the following features that previous studies implicated in affecting

175   mRNA stability: 3' UTR length, 5' UTR length, CDS length, 3' UTR GC content, 5' UTR GC

176   content, CDS GC content, AU rich elements (ARE), miRNA binding sites, number of exons in

177   the transcript, and upstream ORFs (Chan et al., 2017; Cheng, Maier, Avsec, Rus, & Gagneur,

178   2017; Sharova et al., 2009). Combined, these features explained 25% of the variation in mRNA

179   stability. To identify which features had the greatest impact on stability, we analyzed the

180   correlation between each individual feature and mRNA stability (Figure 2B). 3' UTR length had

181   the greatest impact and was negatively correlated with mRNA stability (Spearman's rho -0.3; P

182   < 2.22*10^-16) (Figure 2C). To validate the impact of 3' UTRs on mRNA stability, we used a

183   dual reporter system that contains a control GFP for normalization and a RFP with a cloned

184   endogenous 3' UTR from 12 representative genes (Figure 2D) (Chaudhury et al., 2014). Flow

185   cytometry analysis of cells expressing the reporter showed that the RFP/GFP ratio correlated

186   well with the mRNA stability of the matching endogenous genes as measured by 4sU-Seq

187   (Figure 2D).

188

189   MiRNAs are one regulatory factor that bind to the 3' UTR of target mRNAs and recruit a

190   complex of proteins that then destabilize the transcripts (Fabian & Sonenberg, 2012; Jonas &

191   Izaurralde, 2015). In ESCs the embryonic stem cell-enriched cell cycle (ESCC) family of

192   miRNAs represent a predominant fraction of all miRNAs in ESCs (Greve, Judson, & Blelloch,

193   2013a; Houbaviy, Murray, & Sharp, 2003a; Marson et al., 2008a). As expected, ESCC miRNA

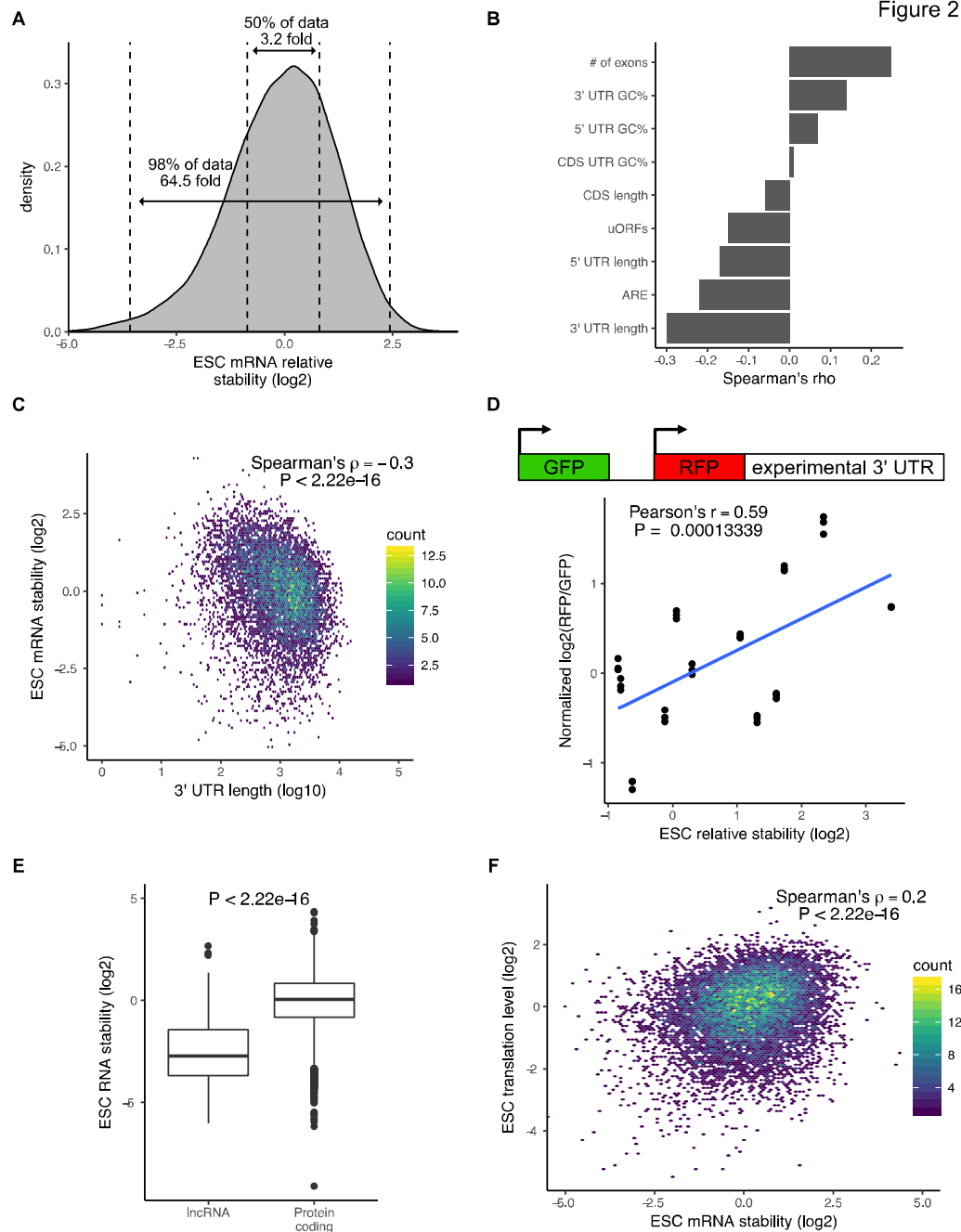194   targets as a group were significantly less stable than all genes (P < 2.22*10^-16, Mann-Whitney

Figure 2

195
196 **Figure 2 There is a wide range of RNA stabilities which are positively correlated with translation**
197 **level in ESCs.**
198 A) The distribution of mRNA stabilities in ESCs. Dashed lines divide bottom 1%, middle 50%, and top 1%
199 of the data. B) The correlation between sequence features and mRNA stability in ESCs. uORFs
200 (upstream open reading frames), ARE (AU Rich Elements). C) The correlation between 3' UTR length
201 (log10) and mRNA stability in ESCs. D) (Top) schematic of dual reporter system to test endogenous 3'
202 UTRs. (Bottom) Normalized median RFP/GFP ratios versus mRNA stability for endogenous genes as
203 measured by 4sU-Seq. Clusters of dots indicate an endogenous 3' UTR, individual dots within a cluster
204 represent biological replicates (n = 3). E) RNA stability of long non-coding RNAs (lncRNAs) compared to
205 protein coding RNAs. P value was calculated using the Mann–Whitney test. F) Comparison between
206 mRNA stability and translation level (high polysome / monosome ratio) in ESCs. P value calculated with
207 correlation significance test. n = 3. See also figure 2 - figure supplement 1.

9

208

209   test) (Figure 2 - figure supplement 1A). However, a large number of ESCC targets were still in

210   the top 50% of the most stable genes (Figure 2 - figure supplement 1A). This data suggests

211   that, while miRNAs are strong destabilizers, they can only explain a small portion of the large

212   range of mRNA stabilities seen in the cells.

213

214   Interestingly, analysis of the 4sU-Seq data showed that long non-coding RNAs (lncRNAs) were

215   significantly less stable than protein coding genes ($P < 2.22*10^{-16}$, Mann-Whitney test) (Figure

216   2E). This result suggested a strong role for translation in regulating RNA stability in ESCs. To

217   further test this hypothesis, we performed polysome profiling (Arava et al., 2003). While both

218   ribosome profiling and polysome profiling measure global levels of translation, polysome

219   profiling enables the measurement of relative elongation time versus initiation time by

220   comparing the fraction of transcripts bound by multiple ribosomes (polysome fraction) versus a

221   single ribosome (monosome fraction) (Heyer & Moore, 2016). Thus, it can be a more sensitive

222   measure of translation regulation. We isolated monosome fractions, low polysome fractions

223   containing 2-4 ribosomes, and high polysome fractions containing 4+ ribosomes and performed

224   RNA-Seq (Figure 2 - figure supplement 1B). To avoid confusion with the translation efficiency

225   metric measured by ribosome profiling, we refer to the ratio of high polysome/monosome as

226   translation levels. As expected, protein coding genes had a much higher translation level

227   compared to lncRNAs ($P < 2.22*10^{-16}$, Mann-Whitney test) (Figure 2 - figure supplement 1C).

228   We next compared the polysome profiling data to the mRNA stability data. There was a highly

229   significant correlation between mRNA stability and translation levels across all genes

230   (Spearman's rho 0.2; $P < 2.22*10^{-16}$) (Figure 2F). These findings suggested a direct link

231   between translation level and mRNA stability.

232

233   Recent reports suggest that differential codon usage is a central mechanism in linking protein

234   translation to mRNA stability (Bazzini et al., 2016; Chan et al., 2017; Cheng et al., 2017;

235   Mishima & Tomari, 2016; Vladimir Presnyak et al., 2015). Therefore, we considered the

236   possibility that codon optimality is a driving force in the wide range of mRNA stabilities. Analysis

237   of the frequency that each codon appears in a transcript uncovered small differences in codon

238   usage frequency when comparing the top and bottom 20% of mRNA stabilities (Figure 2 - figure

239   supplement 1D). Therefore, codon optimality may in part explain the link between translation

240   levels and mRNA stability.

241

242   **DDX6 regulates proliferation and morphology of ESCs.**

243   In yeast, the protein DHH1 has been shown to link translation to mRNA stability through codon

244   optimality (Radhakrishnan et al., 2016). The mammalian homolog of DHH1, DDX6, has been

245   shown to associate with both the mRNA decapping and deadenylation complex, also consistent

246   with a potential link between mRNA stability and translation (Y. Chen et al., 2014b; Mathys et

247   al., 2014b; Rouya et al., 2014b). Therefore, we next asked whether DDX6 may provide a

248   mechanistic link for the relationship between translation and mRNA stability in ESCs. To

249   investigate the function of DDX6 in ESCs, we produced *Ddx6* knockout (*Ddx6* KO) clones using

250   CRISPR-Cas9. Sanger sequencing confirmed a single nucleotide insertion in one clone and a

251   large deletion in a second clone, both of which produce a premature stop (Figure 3 - figure

252   supplement 1A). Western blot confirmed the absence of DDX6 protein in both clones (Figure

253   3A). We repeated the 4sU-Seq and polysome profiling in *Ddx6* KO and matched wild type cells

254   to measure changes in mRNA stability and translation. 4sU-Seq and total RNA-Seq showed that

255   while there was a minimal reduction of nascent *Ddx6* mRNA, there was a drastic loss of mature

256   *Ddx6* mRNA in the *Ddx6* KO cells (Figure 3B). This destabilization is consistent with nonsense

257   mediated decay and further validates the 4sU-Seq assay for assessing changes in mRNA
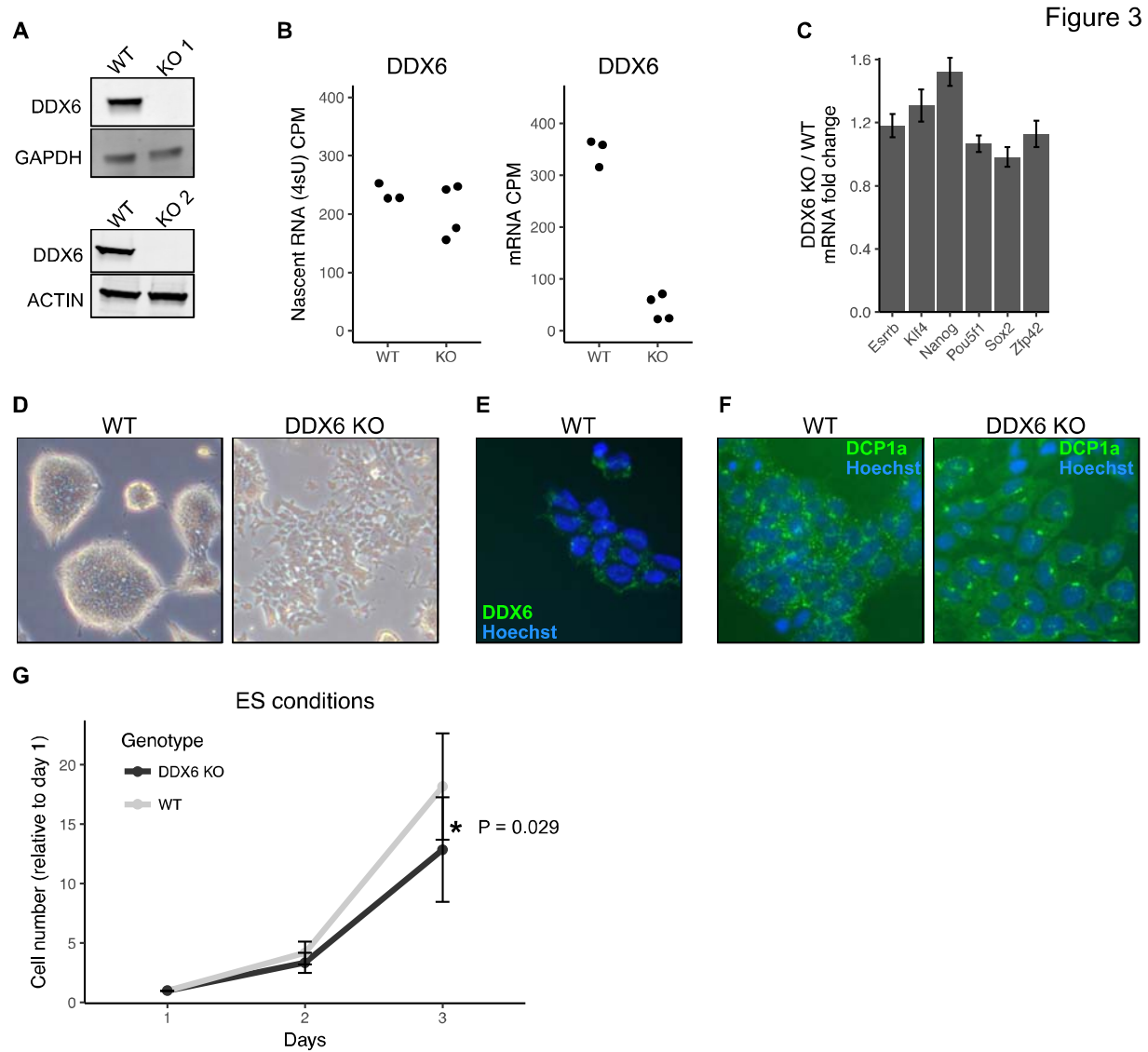
258   stability.

11

Figure 3 DDX6 regulates proliferation and morphology of ESCs.
A) Western blot of DDX6 in two DDX6 knockout lines. GAPDH and ACTIN were used as loading controls. B) *Ddx6* counts per million (CPM) in nascent mRNA (4sU) or mRNA in wild type (WT) and *Ddx6* KO cells. n = 3 for wild type, n = 4 for *Ddx6* KO (2 replicates of each *Ddx6* KO line) C) Expression of pluripotency genes in *Ddx6* KO ESCs based on RNA-Seq. Error bars represent 95% confidence interval. D) Brightfield images of wild type and *Ddx6* KO ESCs. Images taken at 20X. E) DDX6 staining in wild type ESCs. Images taken at 20X. F) P-body staining against DCP1a in wild type and *Ddx6* KO ESCs. Images taken at 20X. G) Growth curves of wild type and *Ddx6* KO ESCs in ESC maintenance conditions (LIF/2i). n = 6 for wild type cells, n = 12 for *Ddx6* KO (6 replicates of each *Ddx6* KO line). * indicates P < 0.05 using a t-test, error bars are standard deviation. See also figure 3 - figure supplement 1.

259

260
261
262
263
264
265
266
267
268
269
270

271

272   The loss of DDX6 had little impact on the expression of pluripotency markers (Figure 3C).

273   However, there were striking morphological changes in the cells (Figure 3D). Unlike wild type

274   ESCs which form tight domed colonies, *Ddx6* KO cells grew in a jagged, dispersed monolayer

275   (Figure 3D). DDX6 localized to discrete punctate in the wild type cells consistent with P-body

276   localization, as previously reported (Figure 3E) (Ernoult-Lange et al., 2012; Hubstenberger et

277   al., 2017; Minshall, Kress, Weil, & Standart, 2009; Vlad Presnyak & Coller, 2013). Interestingly,

278   the loss of DDX6 resulted in an abnormal distribution of the P-body marker DCP1a, suggesting

279   a role for DDX6 P-body formation in ESCs (Figure 3F). DDX6 loss also led to a reduction in

280   proliferation in self-renewal culture conditions (Figure 3G). Together, these data show an

281   important role for DDX6 in retaining normal cell morphology and proliferation.

282

283   **DDX6 separates miRNA-induced translation repression from RNA degradation**

284   Since yeast DHH1 destabilizes lowly translated transcripts enriched in non-optimal codons, we

285   expected that lowly translated genes might be stabilized in *Ddx6* KO ESCs (Radhakrishnan et

286   al., 2016). However, there was minimal correlation between mRNA stability changes in *Ddx6*

287   KO ESCs and wild type translation levels (Spearman's rho -0.11; P < 2.22*10^-16) (Figure 4 -

288   figure supplement 1A). The stabilized transcripts were not specifically enriched within the lowly

289   translated transcripts and instead they occurred across all levels of translation. These data

290   suggested that DDX6 does not link mRNA stability with translation across all genes. Next, we

291   defined a set of codons as suboptimal based on their enrichment in unstable genes in wild type

292   ESCs and asked whether they are enriched among genes that are stabilized in *Ddx6* KO cells

293   (Figure 2 - figure supplement 1D). There was no enrichment (Figure 4 - figure supplement 1B).

294   Further comparing changes in median codon frequency in stable versus unstable transcripts in

295   wild type cells with changes in median codon frequency in stabilized versus unstabilized

296   transcripts in *Ddx6* KO cells showed no correlation (Figure 4 - figure supplement 1C). Species

297   specific tRNA adaptation index (sTAI) provides an alternative metric of codon optimality. The

298   sTAI metric takes into account tRNA copy number and a tRNA's ability to wobble base pair with

299   different codons (Radhakrishnan et al., 2016; Sabi & Tuller, 2014). We calculated sTAI values

300   for mouse and asked if they could predict changes in transcript stability associated with DDX6

301   loss. In contrast to the yeast homolog, transcripts stabilized upon DDX6 loss did not correlate

302   with low sTAI values (Figure 4 - figure supplement 1D). These data show that unlike yeast

303   DHH1, the primary function of mammalian DDX6 is not to link codon optimality with transcript

304   stability.

305

306   Several aspects of the *Ddx6* KO phenotype, including the cell morphology changes and growth

307   defects, resemble the phenotype of *Dgcr8* KO cells (Wang, Medvid, Melton, Jaenisch, &

308   Blelloch, 2007). DGCR8 is essential for miRNA biogenesis and *Dgcr8* KO ESCs lack all

309   miRNAs (Wang et al., 2007). DDX6 has been implicated as an effector of miRNA activity (Y.

310   Chen et al., 2014b; Chu & Rana, 2006; Mathys et al., 2014b; Rouya et al., 2014b). Therefore,

311   we next asked whether *Ddx6* KO cells have similar downstream molecular consequences as

312   *Dgcr8* KO cells. To directly compare the two, we performed 4sU-Seq and polysome profiling in

313   *Dgcr8* KO ESCs and analyzed the data in parallel with that of the *Ddx6* KO ESCs.

314

315   The embryonic stem cell enriched cell cycle (ESCC) family of miRNAs represent a predominant

316   fraction of all miRNAs in ESCs (Greve, Judson, & Blelloch, 2013b; Houbaviy, Murray, & Sharp,

317   2003b; Marson et al., 2008b; Melton, Judson, & Blelloch, 2010; Wang et al., 2008). They share

318   the "AAGUGC" seed sequence and thus have common downstream targets. Furthermore, re-

319   introduction of a single member of the ESCC family of miRNAs can revert *Dgcr8* KO cells to a

320   molecular phenotype highly similar to wild type ESCs (Gambardella et al., 2017; Melton et al.,

321   2010; Wang et al., 2008). Therefore, we chose to focus on the consequence of DGCR8 loss

322   and DDX6 loss on these targets. As expected, the ESCC targets are stabilized relative to all

323   genes in the *Dgcr8* KO cells (Figure 4A). However, these same targets showed little change in
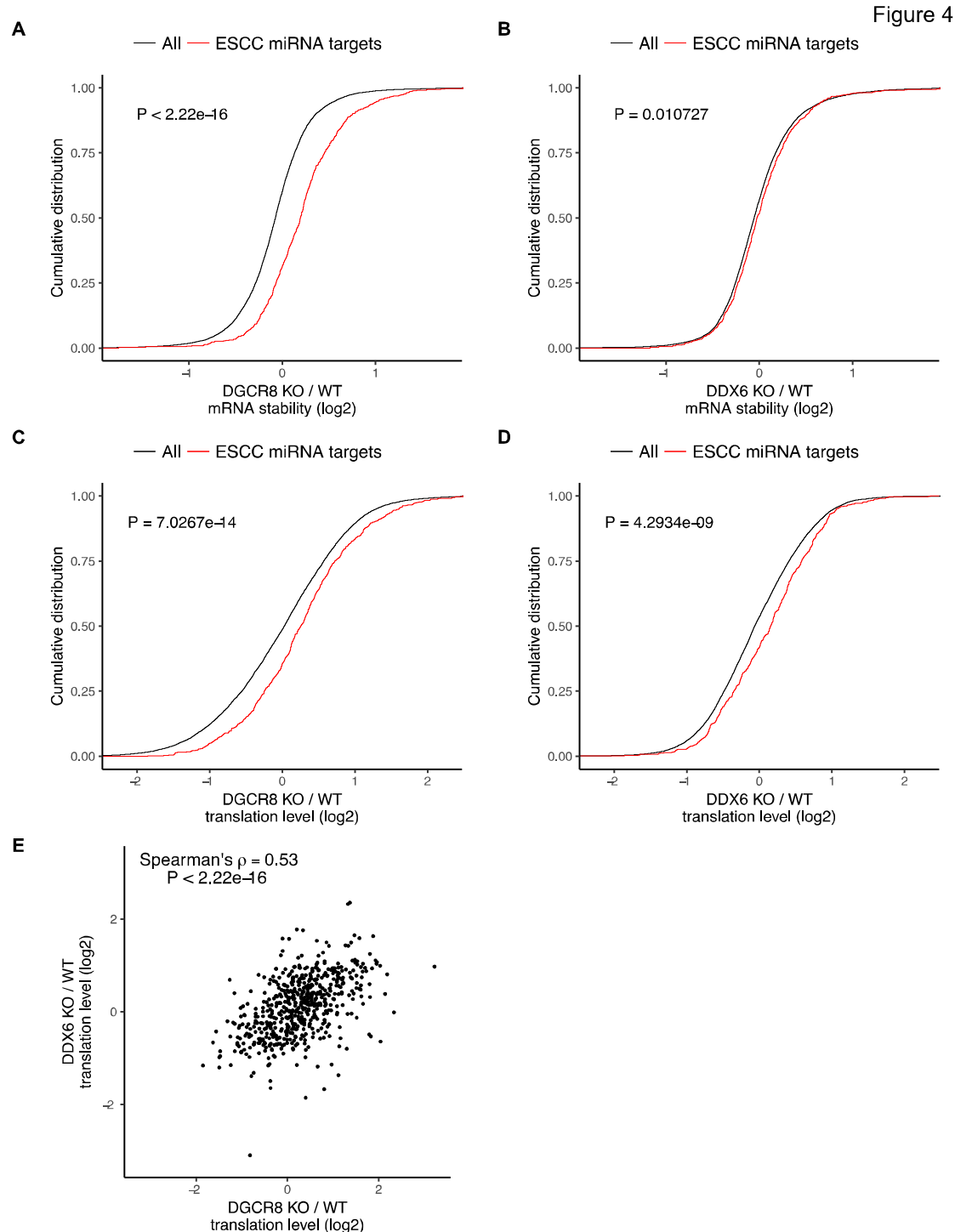
324

Figure 4 DDX6 separates miRNA-induced translation repression from RNA degradation.
A-D) mRNA stability or translation level changes in ESCC miRNA targets versus all mRNAs. P value calculated with Mann-Whitney test. A/B) mRNA stability changes in *Dgcr8* KO (A) or *Ddx6* KO (B) cells. n = 3 for wild type, n = 4 for *Ddx6* KO (2 replicates of each *Ddx6* KO line), n = 3 for *Dgcr8* KO. C/D) Translation level changes in *Dgcr8* KO (C) or *Ddx6* KO (D) cells. n = 3 for each genotype. E) Translation level changes of individual ESCC miRNA targets in *Dgcr8* KO and *Ddx6* KO ESCs. See also figure 4 - figure supplement 1.

332   mRNA stability in the *Ddx6* KO cells (Figure 4B). Therefore, DDX6 does not appear to play a

333   major role in transcript destabilization downstream of miRNAs.

334

335   The loss of DGCR8 also resulted in an increase in translation of ESCC miRNA targets

336   independent of its effect on stability, consistent with miRNAs both inhibiting translation and

337   destabilizing transcripts (Figure 4C). In contrast to the stability data, the loss of DDX6 had a

338   similar impact as the loss of DGCR8 on the translation of ESCC targets (Figure 4D). Indeed,

339   *Dgcr8* KO and *Ddx6* KO affected the translation of individual targets to a similar extent (Figure

340   4E). These data show that DDX6 is an essential effector for miRNA driven translational

341   repression, but not mRNA stabilization. As such, DDX6 separates the two main functions of

342   miRNAs showing that miRNA driven translational repression and transcript destabilization are

343   not dependent on one another.

344

345   **Translational repression alone underlies many of the downstream molecular changes**

346   **associated with miRNA loss**

347   Whether translational repression or mRNA destabilization is the predominant effect of miRNAs

348   is controversial as it is difficult to separate the two (Iwakawa & Tomari, 2015; Jonas &

349   Izaurralde, 2015). Given that the *Ddx6* KO cells retained mRNA destabilization, while losing

350   translational repression of miRNA targets, we asked how well derepression of translation

351   matches the downstream consequences of losing all miRNAs. Since the *Ddx6* KO and *Dgcr8*

352   KO cells have partially overlapping phenotypes, we compared global changes in mRNA stability,

353   mRNA levels, and translation levels. Strikingly, while there was little correlation in changes in

354   mRNA stability, changes in both mRNA and translation levels were well correlated (Figure 5).

355   The correlation in mRNA changes is likely due to transcriptional secondary effects due to losing

356   translation repression of miRNA targets in *Ddx6* KO and *Dgcr8* KO cells. These data show that

357   translational repression alone can explain much of a miRNA's function in ESCs.
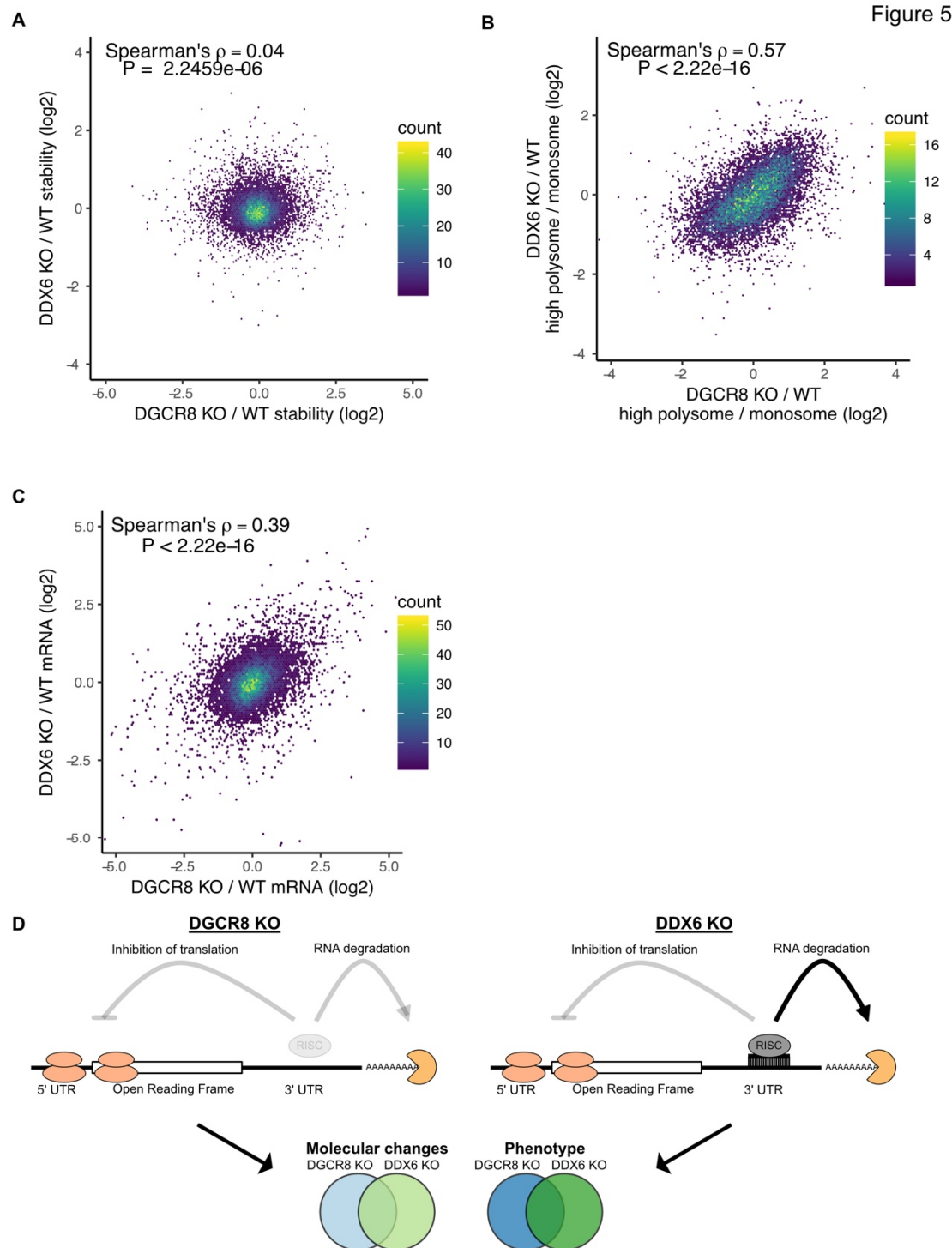
16

Figure 5 Translational repression alone underlies many of the downstream molecular changes associated with miRNA loss.

A) Comparison between mRNA stability changes in *Dgcr8* KO versus *Ddx6* KO cells. n = 3 for wild type, n = 4 for *Ddx6* KO (2 replicates of each *Ddx6* KO line), n = 3 for *Dgcr8* KO. B) Comparison between translation level changes in *Dgcr8* KO versus *Ddx6* KO cells. n = 3 for each genotype. C) Comparison between mRNA changes in *Dgcr8* KO versus *Ddx6* KO cells. P value calculated with correlation significance test. D) Summary schematic comparing *Dgcr8* KO cells to *Ddx6* KO cells.

17

366 **DISCUSSION**

367 In this study we sought to uncover how mRNA stability and translation are regulated within the

368 ESC state and during differentiation. Using RNA-Seq, metabolic labeling (4sU-Seq), and

369 ribosome profiling, we found that most changes during ESC differentiation are driven at the level

370 of transcription. This finding contrasts Lemischka and colleagues' conclusion that post-

371 transcriptional changes underlie many changes in protein levels during ESC differentiation (Lu

372 et al., 2009a). These differences are likely explained by the different approaches used and the

373 fact that Lemischka and colleagues focused their analysis on nuclear protein changes.

374 Discordant changes between mRNA expression and nuclear protein levels could reflect

375 changes in translation levels, protein stability, or protein localization (Liu, Beyer, & Aebersold,

376 2016). We measured translation levels, but not post-translational events; therefore, it remains

377 plausible that protein degradation rates or protein localization are dynamic during ESC

378 differentiation.

379

380 We found a positive correlation between mRNA stability and translation levels in ESCs, similar

381 to what other groups have observed recently in yeast (Chan et al., 2017; Heyer & Moore, 2016;

382 Vladimir Presnyak et al., 2015). A number of mechanisms have been proposed. One is that

383 ribosomes sterically hinder the degradation machinery from accessing the transcript. In support

384 of this model, RNA-Seq of the 5' end of decapped RNA degradation intermediates shows a

385 three nucleotide periodicity consistent with exonucleases running into the ribosome on a final

386 round of translation (Pelechano, Wei, & Steinmetz, 2015). Alternatively, some RNA-binding

387 proteins may sense slowly translating transcripts and accelerate their degradation as recently

388 described for DHH1 (Radhakrishnan et al., 2016). However, in our data the loss of the

389 mammalian homolog of DHH1, DDX6, did not appear to link low levels of translation with low

390 mRNA stability.

391

18

392   There has been extensive debate about whether miRNAs primarily inhibit translation or induce

393   destabilization of their target transcripts (Iwakawa & Tomari, 2015; Jonas & Izaurralde, 2015).

394   By analyzing stability changes and translation changes in *Dgcr8* KO ESCs, which lack all

395   mature miRNAs, we observe that miRNAs both inhibit translation and induce destabilization

396   within ESCs. However, upon loss of DDX6, miRNA targets are derepressed at the translational

397   level without affecting miRNA induced destabilization. It has been suggested that translational

398   repression of miRNA targets is the cause of mRNA destabilization or is at least a prerequisite

399   (Radhakrishnan & Green, 2016). However, the *Ddx6* KO cells demonstrate that mRNA

400   destabilization can occur without translational repression in a context where both forms of

401   repression normally occur. Future studies will likely identify factors that can decouple

402   translational repression and mRNA destabilization in the other direction so that miRNA targets

403   are translationally repressed without inducing mRNA destabilization. This situation has been

404   observed in the early zebrafish embryo, but the mechanism underlying the phenomenon

405   remains unclear (Bazzini et al., 2012).

406

407   Our data supports a key role for DDX6 in the translational repression of miRNA targets.

408   However, it is not fully understood how DDX6 represses translation of these targets.

409   Experiments using DDX6 tethered to different reporters suggest that DDX6 suppresses

410   translational initiation (Kuzuoğlu-Öztürk et al., 2016b). It was recently shown that DDX6

411   interacts with 4E-T, which competes with eIF4G for binding to the translation initiation factor

412   eIF4E and leads to translational repression (Kamenska et al., 2016; Ozgur et al., 2015).

413   Additionally, mutations in the FDF binding domain of DDX6 prevents interaction with 4E-T and

414   decapping proteins and prevents translational repression of a reporter (Kuzuoğlu-Öztürk et al.,

415   2016c). However, depletion of 4E-T only partially alleviates DDX6 mediated translational

416   repression (Kamenska et al., 2014; Kuzuoğlu-Öztürk et al., 2016c). Therefore, DDX6 likely

417   interacts with additional unknown factors to inhibit translation initiation. Our data shows that the

418   loss of DDX6 results in increased translation of miRNA targets to a similar level as the loss of all

419   miRNAs, suggesting that DDX6 serves as a key link between the proteins that repress

420   translation and the rest of the RNA induced silencing complex.

421

422   Surprisingly, we found that *Dgcr8* KO and *Ddx6* KO have similar overall downstream molecular

423   consequences, even though the former leads to both stabilization and translational derepression

424   of miRNA targets, while the later only influences translation. Furthermore, *Ddx6* KO and *Dgcr8*

425   KO cells both display morphology defects and proliferation defects. It has been argued that

426   mRNA changes are the dominant effect of miRNAs, since miRNA induced changes in mRNA

427   levels are often larger than changes in translation efficiency (Eichhorn et al., 2014b; Guo,

428   Ingolia, Weissman, & Bartel, 2010b). However, our data suggests that while miRNAs often have

429   a significant effect on mRNA stability, their impact on translational alone can recapitulate a large

430   portion of the downstream molecular and phenotypic effects associated with miRNA loss.

431

432   **MATERIALS AND METHODS**

433

434   **Gene accession**

435   The accession number for the sequencing data reported in this paper is GEO: GSE112767.

436

437   **4sU-Sequencing**

438   Samples were labeled with 500uM 4-thiouridine (4sU) (Sigma) for 30 minutes then extracted

439   with TRIzol (Invitrogen) and split into two groups. rRNA was depleted from Total RNA using the

440   Ribo-Zero Gold kit (Illumina). 80 ug of RNA was biotinylated according to the following protocol

441   Radle et al. (Rädle et al., 2013). Biotinylated 4sU RNA was isolated and washed using M-270

442   Streptavidin Dynabeads (Invitrogen), eluted with 100mM DTT, and cleaned up with Rneasy

443   minelute columns (Qiagen).

20

444 Libraries were generated with the KAPA Stranded RNA-Seq or Stranded HyperPrep library prep

445 kit (Kapa) and sequenced with single-end 50bp reads. Additional rounds of *Ddx6* KO and

446 matched wild type 4sU samples were sequenced with paired-end reads and counts were

447 merged with single end reads.

448

449 **Cell culture and differentiation**

450 ESCs were grown in Knockout DMEM (Invitrogen) supplemented with 15% Fetal Bovine Serum,

451 LIF and 2i (PD0325901 and CHIR99021). In order to generate EpiLCs, 400,000 ESCs were

452 plated in a 15cm plate; 24 hours later LIF/2i media was removed, cells were washed with PBS,

453 and EpiLCs were collected ~ 56 hours later (Krishnakumar et al., 2016). Cells were tested to be

454 free of mycoplasma.

455

456 **Quant Seq**

457 QuantSeq 3' end counting was used for polysome profiling samples as well as matched wild

458 type, *Ddx6* KO, and *Dgcr8* KO mRNA samples (Figure 4F). RNA was isolated using Rneasy

459 Micro kits (Qiagen). RNA-Seq libraries were generated using the QuantSeq 3' FWD kit

460 (Lexogen) and sequenced with single-end 50bp reads.

461

462 **Ribosome profiling**

463 ESCs and EpiLCs were grown as above. Ribosome profiling libraries were generated using the

464 TruSeq Ribosome Profiling kit (Illumina) and sequenced with single-end 50bp reads. 3

465 nucleotide periodicity of ribosome profiling reads was checked using RiboTaper (Calviello et al.,

466 2016). Adapters were trimmed using cutadapt version 1.14 with the following settings: --

467 minimum-length 26 –maximum-length 32 for the ribosome protected fragments or –minimum-

468 length 32 for the total RNA. Adapater sequence used for trimming:

469 AGATCGGAAGAGCACACGTCT. Reads were mapped with STAR version 2.5.3a to the

21

470   mm10/Gencode M14 genome with the following settings: --outFilterMultimapNmax 1 –

471   outFilterMismatchNoverReadLmax 0.05 –seedSearchStartLmax 13 –winAnchorMultimapNmax

472   200.

473

474   **Polysome Profiling**

475   Two plates of 6 million ESCs were seeded in a 15 cm plate 48 hours prior to collection. Cells

476   were incubated with 100 ug/ml cycloheximide (Sigma) for 2 minutes and then moved to ice.

477   Cells were washed and scraped in PBS with cycloheximide, spun down, and then lysed. Lysate

478   was loaded onto a 10-50% sucrose gradient and centrifuged at 35,000 RPM for 3 hours.

479   Gradients were collected on a gradient station (Biocomp). For each sample, the monosome, low

480   polysome (2-4 ribosomes), and high polysome (4+ ribosomes were collected). RNA was

481   extracted from gradient fractions with TRIzol LS (Invitrogen) and concentrated with the Zymo

482   Clean and Concentrator-5 kit (Zymo) prior to library preparation with the QuantSeq 3' FWD kit

483   (Lexogen).

484

485   **Western blot**

486   Cells were collected in RIPA buffer with Protease Inhibitor Cocktail (Roche). Protein was run on

487   a 4-15% gel (Bio-Rad) then transferred onto a PVDF membrane. Membranes were blocked with

488   Odyssey blocking buffer, blotted with primary and secondary antibodies, and then imaged on

489   the Odyssey imaging system (LI-COR). Antibodies: DDX6 1:1000 (A300-460A-T), GAPDH

490   1:1000 (SC 25778), ACTIN 1:1000 (A4700).

491

492   **Actinomycin D RT-qPCR**

493   Cells were treated with 5 ug/ml Actinomycin D. 0, 2, 4, 6, 8, and 12 hours after treatment, RNA

494   was collected in TRIzol (Invitrogen). Reverse transcription was performed with the Maxima first

495   strand synthesis kit (Thermo Scientific). qPCR was then performed with the SensiFAST SYBR

496   Hi-ROX kit (Bioline) on an ABI 7900HT 384-well PCR machine. Each sample was normalized to

497   18S rRNA and its 0 hour time point.

498

Differentiation RT-qPCR

500   Cells were differentiated to an EpiLC state as described above, scaled down to a 6 well dish.

501   Samples were collected in TRIzol (Invitrogen). Reverse transcription was performed with the

502   Maxima first strand synthesis kit (Thermo Scientific). qPCR was then performed with the

503   SensiFAST SYBR Hi-ROX kit (Bioline) on an ABI 7900HT 384-well PCR machine. Each sample

504   was normalized to Gapdh and wild type ESCs in LIF/2i conditions.

505

BAX/BAK RT-qPCR

507   Cells were collected in TRIzol (Invitrogen) and RNA was isolated using the Directzol miniprep kit

508   (Zymo). qPCR was then performed with the SensiFAST SYBR Hi-ROX kit (Bioline) on an ABI

509   7900HT 384-well PCR machine. Each sample was normalized to Gapdh and the parental

510   BAX/BAK cell line.

511

Cell count

513   50,000 cells were plated in multiple wells of a 6 well on day 0. On day 1, 2, and 3 cells were

514   trypsinized and counted with a TC20 (Bio-rad). Day 2 and 3 counts were normalized to the day

515   1 count.

516

Imaging

518   Cells were fixed with 4% PFA 10 minutes at room temperature. Cells were blocked with 2%

519   BSA and 1% goat serum in PBST. Cells were incubated with primary antibody for 1 hour at

520   room temperature (Dcp1 abcam (ab47811) antibody 1:800 or DDX6 A300-460A) antibody

23

521   1:250). Cells were incubated with goat 488 secondary for 1 hour at room temperature. Cells

522   were then imaged on a Leica inverted fluorescence microscope.

523

524   **Generation of *Ddx6* KO ESCs**

525   *Ddx6* KO lines were generated using the protocol from Ran et al. (Ran et al., 2013). A guide

526   RNA (CATGTGGTGATCGCTACCCC) was cloned into PX458, transfected into ESCs using

527   Fugene 6, and then GFP positive cells were sorted at clonal density. Clones were genotyped

528   with the following primers (Fwd: CATTGCCCAGATTGAAGACA and Rvs:

529   TCCTGACTGGCCTGAAACTT) and verified by western blot. Two different knockout clones

530   were picked and used for all subsequent analysis.

531

532   **Species specific tRNA adaptation index calculation**

533   For each gene, the CDS region from the Gencode M14 annotation was used. Species specific

534   tRNA adaptation index (sTAI) values for each gene were calculated with stAIcalc (Sabi,

535   Volvovitch Daniel, & Tuller, 2017).

536

537   **Calculation of codon usage**

538   For each gene, the APPRIS principle isoform was used to calculate codon usage frequency. To

539   analyze differences in codon usage between stable and unstable genes, codon usage

540   frequency was calculated for genes in the top 20% (stable) and bottom 20% (unstable) in terms

541   of wild type mRNA stability. For codon usage frequency for mRNA stability changes in *Ddx6* KO

542   cells, we first filtered for genes in the bottom 20% of wild type stability as defined above. Within

543   those genes, we took the top 20% (top) and bottom 20% (bottom) of mRNA stability changes in

544   *Ddx6* KO ESCs and calculated codon usage frequency within each group. For the comparison

545   between codon usage frequency in wild type versus *Ddx6* KO, we took the median codon usage

546   frequency in stable – the median codon usage frequency in unstable for each codon and

547   compared it to the *Ddx6* KO median codon usage frequency in the bottom group – median

548   codon usage frequency in the top group, using groups as defined above.

549

550   **Analysis software**

551   For all samples, adapters were trimmed with Cutadapt version 1.14 with the following options: -

552   m 20 -a "A{18}" -a "T{18}" -a AGATCGGAAGAGCACACGTCTGAACTCCAGTCAC. Reads were

553   mapped with STAR version 2.5.3a to the mm10/Gencode M14 genome with the following

554   settings: --outFilterMultimapNmax 1 –outFilterMismatchNoverReadLmax 0.05 –

555   seedSearchStartLmax 25 –winAnchorMultimapNmax 100. Reads were counted with

556   featureCounts version 1.5.3 using the Gencode M14 annotation with rRNA annotations removed

557   with the following settings: -s. Differential expression was carried out with limma version 3.32.10

558   and R version 3.4.2. Genes with a low number of reads were filtered out: a gene must have at

559   least 3 counts per million across at least 3 replicates to be included for differential expression.

560   For samples with multiple comparisons, a linear model was used for each condition in limma

561   taking into account assay type (e.g. 4sU versus total RNA) and cell type (e.g. KO versus wild

562   type); significant changes in stability or translation are based on the interaction term. All

563   downstream analysis was performed in R version 3.4.2 and plotted with ggplot2.

564

565   **Polysome Profiling Analysis**

566   RNA-Seq from the monosome, low polysome (2-4 ribosomes), and high polysome (4+

567   ribosomes were collected) fractions was mapped as above. Translation level was defined as the

568   ratio of the high polysome counts divided by the monosome counts. For KO versus wild type

569   analysis, a linear model was used for each condition in limma and significant changes in

570   translation are based on the interaction term.

571

572   **4sU-Seq Analysis**

573   By measuring transcription rate and steady state mRNA levels, it is possible to infer the relative

574   degradation rate (Rabani et al., 2011). It is assumed that across the population of cells there is

575   no change in mRNA levels over time for a given state. Therefore, changes mRNA levels can be

576   modeled by their production rate α and degradation rate β.

$$dmRNA/dt \ = \ \alpha - \beta[mRNA] \ \approx \ 0$$

577   Solving for this equation, degradation rates can be calculated using a production rate (in this

578   case nascent RNA transcription as measured by 4sU incorporation) and the concentration of

579   total mRNA in the cell (as measured by total RNA-Seq).

580   $\alpha/[mRNA] \ \approx \ \beta.$

581   For KO versus wild type analysis, a linear model was used for each condition in limma and

582   significant changes in translation are based on the interaction term.

583

584   **Analysis of features regulating RNA stability**

585   For each gene with multiple isoforms, the APPRIS principle isoform was used. APPRIS data

586   were downloaded on 10/30/2017. Log10(feature lengths), GC %, and number of exons were

587   calculated in R version 3.4.2. Upstream open reading frames were defined as the number of

588   ATG sequences in the 5' UTR. AU rich elements were defined as the number of UAUUUAU

589   sequences in the 3' UTR. miRNA sites were defined as below. Each of these features and

590   mRNA stability were used in a multiple linear regression using the lm function in R version 3.4.2.

591   Additionally, the Spearman correlation was calculated between each feature and mRNA

592   stability.

593

594   **microRNA targets**

595   Conserved microRNA targets were downloaded from Targetscan mouse release 7.1. This list

596   was filtered for genes that are targeted by the miR-291-3p/294-3p/295-3p/302-3p family yielding

597   765 target genes.

26

598

3' UTR analysis

599

600   For each gene, the APPRIS principle isoform was used to calculate log10 (3' UTR length).

601   Log10(3' UTR length) was then compared to log2 relative mRNA stability.

602

3' UTR reporters

603

604   Endogenous 3' UTRs from the following genes were amplified from ESC cDNA:

605   ENSMUSG00000021583, ENSMUSG00000029580, ENSMUSG00000043716,

606   ENSMUSG00000010342, ENSMUSG00000021665, ENSMUSG00000024406,

607   ENSMUSG00000052911, ENSMUSG00000058056, ENSMUSG00000020105,

608   ENSMUSG00000026003, ENSMUSG00000020038, ENSMUSG00000025521,

609   ENSMUSG00000031503. Genes were cloned into the pBUTR (piggyBac-based 3′ UnTranslated

610   Region reporter) using gateway cloning as outlined in Chaudhury et al (Chaudhury et al., 2014).

611   Reporters were transfected into ESCs using Fugene 6 (Promega). Cells were treated with

612   Geneticin to enrich for transfected cells. Cells were analyzed on an LSRII (BD). RFP+/GFP+

613   cells were gated in FlowJo and median RFP/GFP ratios were calculated. RFP/GFP ratios were

614   standardized between days to accounts for differences in laser power.

615

Primers

616

		Forward	Reverse
Gapdh (JF207/208)	Gapdh	AGGTCGGTGTGAACGGATTTG	TGTAGACCATGTAGTTGAGGTCA
Nanog (JF325/326)	Nanog	AACCAAAGGATGAAGTGCAAGCGG	TCCAAGTTGGGTTGGTCCAAGTCT
JF_AC-Zfp42	Zfp42	CTCCTGCACACAGAAGAAAGC	CACTGATCCGCAAACACC
JF_AC-Fgf5	Fgf5	CCTTGCGACCCAGGAGCTTA	CCGTCTGTGGTTTCTGTTGAGG
JF_AC-Otx2	Otx2	CAACTTGCCAGAATCCAGGG	GGCCTCACTTTGTTCTGACC
JF 371/372	Bak	gctgacatgtttgctgatgg	gatcagctcgggcactttag
JF 323/324	Ddx6 qPCR	ACTATACTCCGCTACTTTCCCTC	TGGCGCTCCGTTACATATG

JF 355/356	18S	GTGGAGCGATTTGTCTGGTT	CGCTGAGCCAGTCAGTGTAG
JF 375/376	MycN	AGTGTGTCTGTTCCAGCTACTG	TTCATCTTCCTCCTCGTCATCC
JF343/344	Pgap1	AGTACCCCGAGTACCAGAAAAT	TCGAACTTGCTTATAGCTTCCAG
JF345/346	Impact	GTGAAGAAATCGAAGCAATGGC	GGTACTCACTTGGCAACATCA
JF347/348	Cyr61	AACGAGGACTGCAGCAAAAC	TTCTGACTGAGCTCTGCAGATC
JF349/350	Amotl2	AGGGACAATGAGCGATTGCAG	CCTCACGCTTGGAAGAGGT
JF293/294	Ddx6 Genotyping	CATTGCCCAGATTGAAGACA	TCCTGACTGGCCTGAAACTT

617

ACKNOWLEDGEMENTS

625

AUTHOR CONTRIBUTIONS

627 J.W.F., and R.B. conceived the study, designed the study, and wrote the manuscript. J.W.F.

628 and T.H. performed experiments.

629

COMPETING INTERESTS

631 The authors declare no competing interests.

632

REFERENCES

634 Arava, Y., Wang, Y., Storey, J. D., Liu, C. L., Brown, P. O., & Herschlag, D. (2003). Genome-

635 wide analysis of mRNA translation profiles in Saccharomyces cerevisiae. *Proceedings of*

636 *the National Academy of Sciences of the United States of America*, *100*(7), 3889–3894.

637 Ayache, J., Bénard, M., Ernoult-Lange, M., Minshall, N., Standart, N., Kress, M., & Weil, D.

638   (2015). P-body assembly requires DDX6 repression complexes rather than decay or

639   Ataxin2/2L complexes. *Molecular Biology of the Cell*, *26*(14), 2579–2595.

640 Bazzini, A. A., del Viso, F., Moreno☐Mateos, M. A., Johnstone, T. G., Vejnar, C. E., Qin, Y., …

641   Giraldez, A. J. (2016). Codon identity regulates mRNA stability and translation efficiency

642   during the maternal☐to☐zygotic transition. *The EMBO Journal*, *35*(19), 2087–2103.

643 Bazzini, A. A., Lee, M. T., & Giraldez, A. J. (2012). Ribosome profiling shows that miR-430

644   reduces translation before causing mRNA decay in zebrafish. *Science*, *336*(6078), 233–

645   237.

646 Beelman, C. A., & Parker, R. (1994). Differential effects of translational inhibition in cis and in

647   trans on the decay of the unstable yeast MFA2 mRNA. *The Journal of Biological*

648   *Chemistry*, *269*(13), 9687–9692.

649 Bensaude, O. (2011). Inhibiting eukaryotic transcription. Which compound to choose? How to

650   evaluate its activity? *Transcription*, *2*(3), 103–108.

651 Béthune, J., Artus-Revel, C. G., & Filipowicz, W. (2012). Kinetic analysis reveals successive

652   steps leading to miRNA-mediated silencing in mammalian cells. *EMBO Reports*, *13*(8),

653   716–723.

654 Boroviak, T., Loos, R., Lombard, P., Okahara, J., Behr, R., Sasaki, E., … Bertone, P. (2015).

655   Lineage-Specific Profiling Delineates the Emergence and Progression of Naïve

656   Pluripotency in Mammalian Embryogenesis. *Developmental Cell*, *35*(3), 366–382.

657 Calviello, L., Mukherjee, N., Wyler, E., Zauber, H., Hirsekorn, A., Selbach, M., … Ohler, U.

658   (2016). Detecting actively translated open reading frames in ribosome profiling data.

659   *Nature Methods*, *13*(2), 165–170.

660 Carroll, J. S., Munchel, S. E., & Weis, K. (2011). The DexD/H box ATPase Dhh1 functions in

661   translational repression, mRNA decay, and processing body dynamics. *The Journal of Cell*

662   *Biology*, *194*(4), 527–537.

663   Chan, L. Y., Mugler, C. F., Heinrich, S., Vallotton, P., & Weis, K. (2017). Non-invasive

664   measurement of mRNA decay reveals translation initiation as the major determinant of

665   mRNA stability. https://doi.org/10.1101/214775

666   Chaudhury, A., Kongchan, N., Gengler, J. P., Mohanty, V., Christiansen, A. E., Fachini, J. M., …

667   Neilson, J. R. (2014). A piggyBac-based reporter system for scalable in vitro and in vivo

668   analysis of 3′ untranslated region-mediated gene regulation. *Nucleic Acids Research*,

669   *42*(10), e86–e86.

670   Chen, A., Liu, A., Krishnakumar, R., Freimer, J., DeVeale, B., & Blelloch, R. (n.d.). Enhancer

671   switching subsets gene networks during the transition from naïve to formative pluripotency.

672   *In Revision*.

673   Cheng, J., Maier, K. C., Avsec, Z., Rus, P., & Gagneur, J. (2016). Cis-regulatory elements

674   explain most of the mRNA stability variation across genes in yeast.

675   https://doi.org/10.1101/085522

676   Cheng, J., Maier, K. C., Avsec, Ž., Rus, P., & Gagneur, J. (2017). -regulatory elements explain

677   most of the mRNA stability variation across genes in yeast. *RNA* , *23*(11), 1648–1659.

678   Chen, Y., Boland, A., Kuzuoğlu-Öztürk, D., Bawankar, P., Loh, B., Chang, C.-T., … Izaurralde,

679   E. (2014a). A DDX6-CNOT1 Complex and W-Binding Pockets in CNOT9 Reveal Direct

680   Links between miRNA Target Recognition and Silencing. *Molecular Cell*, *54*(5), 737–750.

681   Chen, Y., Boland, A., Kuzuoğlu-Öztürk, D., Bawankar, P., Loh, B., Chang, C.-T., … Izaurralde,

682   E. (2014b). A DDX6-CNOT1 Complex and W-Binding Pockets in CNOT9 Reveal Direct

683   Links between miRNA Target Recognition and Silencing. *Molecular Cell*, *54*(5), 737–750.

684   Chu, C.-Y., & Rana, T. M. (2006). Translation repression in human cells by microRNA-induced

685   gene silencing requires RCK/p54. *PloS Biology*, *4*(7), e210.

686   Coller, J., & Parker, R. (2005). General translational repression by activators of mRNA

687   decapping. *Cell*, *122*(6), 875–886.

688   Djuranovic, S., Nahvi, A., & Green, R. (2012). miRNA-mediated gene silencing by translational

689   repression followed by mRNA deadenylation and decay. *Science*, *336*(6078), 237–240.

690   Dolken, L., Ruzsics, Z., Radle, B., Friedel, C. C., Zimmer, R., Mages, J., … Koszinowski, U. H.

691   (2008). High-resolution gene expression profiling for simultaneous kinetic parameter

692   analysis of RNA synthesis and decay. *RNA* , *14*(9), 1959–1972.

693   Eichhorn, S. W., Guo, H., McGeary, S. E., Rodriguez-Mias, R. A., Shin, C., Baek, D., … Bartel,

694   D. P. (2014a). mRNA destabilization is the dominant effect of mammalian microRNAs by

695   the time substantial repression ensues. *Molecular Cell*, *56*(1), 104–115.

696   Eichhorn, S. W., Guo, H., McGeary, S. E., Rodriguez-Mias, R. A., Shin, C., Baek, D., … Bartel,

697   D. P. (2014b). mRNA destabilization is the dominant effect of mammalian microRNAs by

698   the time substantial repression ensues. *Molecular Cell*, *56*(1), 104–115.

699   Ernoult-Lange, M., Baconnais, S., Harper, M., Minshall, N., Souquere, S., Boudier, T., … Weil,

700   D. (2012). Multiple binding of repressed mRNAs by the P-body protein Rck/p54. *RNA* ,

701   *18*(9), 1702–1715.

702   Fabian, M. R., & Sonenberg, N. (2012). The mechanics of miRNA-mediated gene silencing: a

703   look under the hood of miRISC. *Nature Structural & Molecular Biology*, *19*(6), 586–593.

704   Gambardella, G., Carissimo, A., Chen, A., Cutillo, L., Nowakowski, T. J., di Bernardo, D., &

705   Blelloch, R. (2017). The impact of microRNAs on transcriptional heterogeneity and gene

706   co-expression across single embryonic stem cells. *Nature Communications*, *8*, 14126.

707   Greve, T. S., Judson, R. L., & Blelloch, R. (2013a). microRNA control of mouse and human

708   pluripotent stem cell behavior. *Annual Review of Cell and Developmental Biology*, *29*, 213–

709   239.

710   Greve, T. S., Judson, R. L., & Blelloch, R. (2013b). microRNA control of mouse and human

711   pluripotent stem cell behavior. *Annual Review of Cell and Developmental Biology*, *29*, 213–

712   239.

713   Guo, H., Ingolia, N. T., Weissman, J. S., & Bartel, D. P. (2010a). Mammalian microRNAs

714   predominantly act to decrease target mRNA levels. *Nature*, *466*(7308), 835–840.

715   Guo, H., Ingolia, N. T., Weissman, J. S., & Bartel, D. P. (2010b). Mammalian microRNAs

716   predominantly act to decrease target mRNA levels. *Nature*, *466*(7308), 835–840.

717   Hasan, A., Cotobal, C., Duncan, C. D. S., & Mata, J. (2014). Systematic analysis of the role of

718   RNA-binding proteins in the regulation of RNA stability. *PloS Genetics*, *10*(11), e1004684.

719   Heyer, E. E., & Moore, M. J. (2016). Redefining the Translational Status of 80S Monosomes.

720   *Cell*, *164*(4), 757–769.

721   Houbaviy, H. B., Murray, M. F., & Sharp, P. A. (2003a). Embryonic Stem Cell-Specific

722   MicroRNAs. *Developmental Cell*, *5*(2), 351–358.

723   Houbaviy, H. B., Murray, M. F., & Sharp, P. A. (2003b). Embryonic Stem Cell-Specific

724   MicroRNAs. *Developmental Cell*, *5*(2), 351–358.

725   Hubstenberger, A., Courel, M., Bénard, M., Souquere, S., Ernoult-Lange, M., Chouaib, R., …

726   Weil, D. (2017). P-Body Purification Reveals the Condensation of Repressed mRNA

727   Regulons. *Molecular Cell*, *68*(1), 144–157.e5.

728   Huch, S., & Nissan, T. (2014). Interrelations between translation and general mRNA

729   degradation in yeast. *Wiley Interdisciplinary Reviews. RNA*, *5*(6), 747–763.

730   Ingolia, N. T., Lareau, L. F., & Weissman, J. S. (2011). Ribosome profiling of mouse embryonic

731   stem cells reveals the complexity and dynamics of mammalian proteomes. *Cell*, *147*(4),

732   789–802.

733   Ivanova, N., Dobrin, R., Lu, R., Kotenko, I., Levorse, J., DeCoste, C., … Lemischka, I. R.

734   (2006). Dissecting self-renewal in stem cells with RNA interference. *Nature*, *442*(7102),

735   533–538.

736   Iwakawa, H.-O., & Tomari, Y. (2015). The Functions of MicroRNAs: mRNA Decay and

737   Translational Repression. *Trends in Cell Biology*, *25*(11), 651–665.

738   Jonas, S., & Izaurralde, E. (2015). Towards a molecular understanding of microRNA-mediated

739   gene silencing. *Nature Reviews. Genetics*, *16*(7), 421–433.

740   Kamenska, A., Lu, W.-T., Kubacka, D., Broomhead, H., Minshall, N., Bushell, M., & Standart, N.

741   (2014). Human 4E-T represses translation of bound mRNAs and enhances microRNA-

742   mediated silencing. *Nucleic Acids Research*, *42*(5), 3298–3313.

743 Kamenska, A., Simpson, C., Vindry, C., Broomhead, H., Bénard, M., Ernoult-Lange, M., …

744   Standart, N. (2016). The DDX6-4E-T interaction mediates translational repression and P-

745   body assembly. *Nucleic Acids Research*, *44*(13), 6318–6334.

746 Krishnakumar, R., Chen, A. F., Pantovich, M. G., Danial, M., Parchem, R. J., Labosky, P. A., &

747   Blelloch, R. (2016). FOXD3 Regulates Pluripotent Stem Cell Potential by Simultaneously

748   Initiating and Repressing Enhancer Activity. *Cell Stem Cell*, *18*(1), 104–117.

749 Kuzuoğlu-Öztürk, D., Bhandari, D., Huntzinger, E., Fauser, M., Helms, S., & Izaurralde, E.

750   (2016a). miRISC and the CCR4-NOT complex silence mRNA targets independently of 43S

751   ribosomal scanning. *The EMBO Journal*, *35*(11), 1186–1203.

752 Kuzuoğlu-Öztürk, D., Bhandari, D., Huntzinger, E., Fauser, M., Helms, S., & Izaurralde, E.

753   (2016b). miRISC and the CCR4-NOT complex silence mRNA targets independently of 43S

754   ribosomal scanning. *The EMBO Journal*, *35*(11), 1186–1203.

755 Kuzuoğlu-Öztürk, D., Bhandari, D., Huntzinger, E., Fauser, M., Helms, S., & Izaurralde, E.

756   (2016c). miRISC and the CCR4-NOT complex silence mRNA targets independently of 43S

757   ribosomal scanning. *The EMBO Journal*, *35*(11), 1186–1203.

758 Liu, Y., Beyer, A., & Aebersold, R. (2016). On the Dependency of Cellular Protein Levels on

759   mRNA Abundance. *Cell*, *165*(3), 535–550.

760 Lugowski, A., Nicholson, B., & Rissland, O. S. (2017). Determining mRNA half-lives on a

761   transcriptome-wide scale. *Methods* . https://doi.org/10.1016/j.ymeth.2017.12.006

762 Lu, R., Markowetz, F., Unwin, R. D., Leek, J. T., Airoldi, E. M., MacArthur, B. D., … Lemischka,

763   I. R. (2009a). Systems-level dynamic analyses of fate change in murine embryonic stem

764   cells. *Nature*, *462*(7271), 358–362.

765 Lu, R., Markowetz, F., Unwin, R. D., Leek, J. T., Airoldi, E. M., MacArthur, B. D., … Lemischka,

766   I. R. (2009b). Systems-level dynamic analyses of fate change in murine embryonic stem

767   cells. *Nature*, *462*(7271), 358–362.

768   Marson, A., Levine, S. S., Cole, M. F., Frampton, G. M., Brambrink, T., Johnstone, S., …

769   Young, R. A. (2008a). Connecting microRNA genes to the core transcriptional regulatory

770   circuitry of embryonic stem cells. *Cell*, *134*(3), 521–533.

771   Marson, A., Levine, S. S., Cole, M. F., Frampton, G. M., Brambrink, T., Johnstone, S., …

772   Young, R. A. (2008b). Connecting microRNA genes to the core transcriptional regulatory

773   circuitry of embryonic stem cells. *Cell*, *134*(3), 521–533.

774   Mathys, H., Basquin, J., Ozgur, S., Czarnocki-Cieciura, M., Bonneau, F., Aartse, A., …

775   Filipowicz, W. (2014a). Structural and biochemical insights to the role of the CCR4-NOT

776   complex and DDX6 ATPase in microRNA repression. *Molecular Cell, 54*(5), 751–765.

777   Mathys, H., Basquin, J., Ozgur, S., Czarnocki-Cieciura, M., Bonneau, F., Aartse, A., …

778   Filipowicz, W. (2014b). Structural and biochemical insights to the role of the CCR4-NOT

779   complex and DDX6 ATPase in microRNA repression. *Molecular Cell*, *54*(5), 751–765.

780   Melton, C., Judson, R. L., & Blelloch, R. (2010). Opposing microRNA families regulate self-

781   renewal in mouse embryonic stem cells. *Nature*, *463*(7281), 621–626.

782   Minshall, N., Kress, M., Weil, D., & Standart, N. (2009). Role of p54 RNA helicase activity and

783   its C-terminal domain in translational repression, P-body localization and assembly.

784   *Molecular Biology of the Cell*, *20*(9), 2464–2472.

785   Mishima, Y., & Tomari, Y. (2016). Codon Usage and 3' UTR Length Determine Maternal mRNA

786   Stability in Zebrafish. *Molecular Cell*, *61*(6), 874–885.

787   Nissan, T., Rajyaguru, P., She, M., Song, H., & Parker, R. (2010). Decapping activators in

788   Saccharomyces cerevisiae act by multiple mechanisms. *Molecular Cell*, *39*(5), 773–783.

789   Ozgur, S., Basquin, J., Kamenska, A., Filipowicz, W., Standart, N., & Conti, E. (2015). Structure

790   of a Human 4E-T/DDX6/CNOT1 Complex Reveals the Different Interplay of DDX6-Binding

791   Proteins with the CCR4-NOT Complex. *Cell Reports*, *13*(4), 703–711.

792   Parchem, R. J., Ye, J., Judson, R. L., LaRussa, M. F., Krishnakumar, R., Blelloch, A., …

793   Blelloch, R. (2014). Two miRNA clusters reveal alternative paths in late-stage

794   reprogramming. *Cell Stem Cell*, *14*(5), 617–631.

795   Parker, R. (2012). RNA Degradation in Saccharomyces cerevisae. *Genetics*, *191*(3), 671–702.

796   Pelechano, V., Wei, W., & Steinmetz, L. M. (2015). Widespread Co-translational RNA Decay

797   Reveals Ribosome Dynamics. *Cell*, *161*(6), 1400–1412.

798   Presnyak, V., Alhusaini, N., Chen, Y.-H., Martin, S., Morris, N., Kline, N., … Coller, J. (2015).

799   Codon optimality is a major determinant of mRNA stability. *Cell*, *160*(6), 1111–1124.

800   Presnyak, V., & Coller, J. (2013). The DHH1/RCKp54 family of helicases: an ancient family of

801   proteins that promote translational silencing. *Biochimica et Biophysica Acta*, *1829*(8), 817–

802   823.

803   Rabani, M., Levin, J. Z., Fan, L., Adiconis, X., Raychowdhury, R., Garber, M., … Regev, A.

804   (2011). Metabolic labeling of RNA uncovers principles of RNA production and degradation

805   dynamics in mammalian cells. *Nature Biotechnology*, *29*(5), 436–442.

806   Radhakrishnan, A., Chen, Y.-H., Martin, S., Alhusaini, N., Green, R., & Coller, J. (2016). The

807   DEAD-Box Protein Dhh1p Couples mRNA Decay and Translation by Monitoring Codon

808   Optimality. *Cell*, *167*(1), 122–132.e9.

809   Radhakrishnan, A., & Green, R. (2016). Connections Underlying Translation and mRNA

810   Stability. *Journal of Molecular Biology*, *428*(18), 3558–3564.

811   Rädle, B., Rutkowski, A. J., Ruzsics, Z., Friedel, C. C., Koszinowski, U. H., & Dölken, L. (2013).

812   Metabolic Labeling of Newly Transcribed RNA for High Resolution Gene Expression

813   Profiling of RNA Synthesis, Processing and Decay in Cell Culture. *JoVE (Journal of*

814   *Visualized Experiments)*, (78), e50195–e50195.

815   Ran, F. A., Hsu, P. D., Wright, J., Agarwala, V., Scott, D. A., & Zhang, F. (2013). Genome

816   engineering using the CRISPR-Cas9 system. *Nature Protocols*, *8*(11), 2281–2308.

817   Rouya, C., Siddiqui, N., Morita, M., Duchaine, T. F., Fabian, M. R., & Sonenberg, N. (2014a).

818   Human DDX6 effects miRNA-mediated gene silencing via direct binding to CNOT1. *RNA* ,

819 *20*(9), 1398–1409.

820 Rouya, C., Siddiqui, N., Morita, M., Duchaine, T. F., Fabian, M. R., & Sonenberg, N. (2014b).

821 Human DDX6 effects miRNA-mediated gene silencing via direct binding to CNOT1. *RNA* ,

822 *20*(9), 1398–1409.

823 Roy, B., & Jacobson, A. (2013). The intimate relationships of mRNA decay and translation.

824 *Trends in Genetics: TIG*, *29*(12), 691–699.

825 Sabi, R., & Tuller, T. (2014). Modelling the efficiency of codon-tRNA interactions based on

826 codon usage bias. *DNA Research: An International Journal for Rapid Publication of*

827 *Reports on Genes and Genomes*, *21*(5), 511–526.

828 Sabi, R., Volvovitch Daniel, R., & Tuller, T. (2017). stAIcalc: tRNA adaptation index calculator

829 based on species-specific weights. *Bioinformatics* , *33*(4), 589–591.

830 Schwanhäusser, B., Busse, D., Li, N., Dittmar, G., Schuchhardt, J., Wolf, J., … Selbach, M.

831 (2011). Global quantification of mammalian gene expression control. *Nature*, *473*(7347),

832 337–342.

833 Schwartz, D. C., & Parker, R. (1999). Mutations in translation initiation factors lead to increased

834 rates of deadenylation and decapping of mRNAs in Saccharomyces cerevisiae. *Molecular*

835 *and Cellular Biology*, *19*(8), 5247–5256.

836 Sharova, L. V., Sharov, A. A., Nedorezov, T., Piao, Y., Shaik, N., & S.H. Ko, M. (2009).

837 Database for mRNA Half-Life of 19 977 Genes Obtained by DNA Microarray Analysis of

838 Pluripotent and Differentiating Mouse Embryonic Stem Cells. *DNA Research: An*

839 *International Journal for Rapid Publication of Reports on Genes and Genomes*, *16*(1), 45–

840 58.

841 Shoemaker, C. J., & Green, R. (2012). Translation drives mRNA quality control. *Nature*

842 *Structural & Molecular Biology*, *19*(6), 594–601.

843 Sweet, T., Kovalak, C., & Coller, J. (2012). The DEAD-box protein Dhh1 promotes decapping by

844 slowing ribosome movement. *PloS Biology*, *10*(6), e1001342.

845   Tritschler, F., Braun, J. E., Eulalio, A., Truffault, V., Izaurralde, E., & Weichenrieder, O. (2009).

846   Structural basis for the mutually exclusive anchoring of P body components EDC3 and Tral

847   to the DEAD box protein DDX6/Me31B. *Molecular Cell*, *33*(5), 661–668.

848   Wang, Y., Baskerville, S., Shenoy, A., Babiarz, J. E., Baehner, L., & Blelloch, R. (2008).

849   Embryonic stem cell-specific microRNAs regulate the G1-S transition and promote rapid

850   proliferation. *Nature Genetics*, *40*(12), 1478–1483.

851   Wang, Y., Medvid, R., Melton, C., Jaenisch, R., & Blelloch, R. (2007). DGCR8 is essential for

852   microRNA biogenesis and silencing of embryonic stem cell self-renewal. *Nature Genetics*,

853   *39*(3), 380–385.

854   Windhager, L., Bonfert, T., Burger, K., Ruzsics, Z., Krebs, S., Kaufmann, S., … Dölken, L.

855   (2012). Ultrashort and progressive 4sU-tagging reveals key characteristics of RNA

856   processing at nucleotide resolution. *Genome Research*, *22*(10), 2031–2042.

857   Wu, X., & Brewer, G. (2012). The regulation of mRNA stability in mammalian cells: 2.0. *Gene*,

858   *500*(1), 10–21.

859

860

861

862

863

864

865

866

867
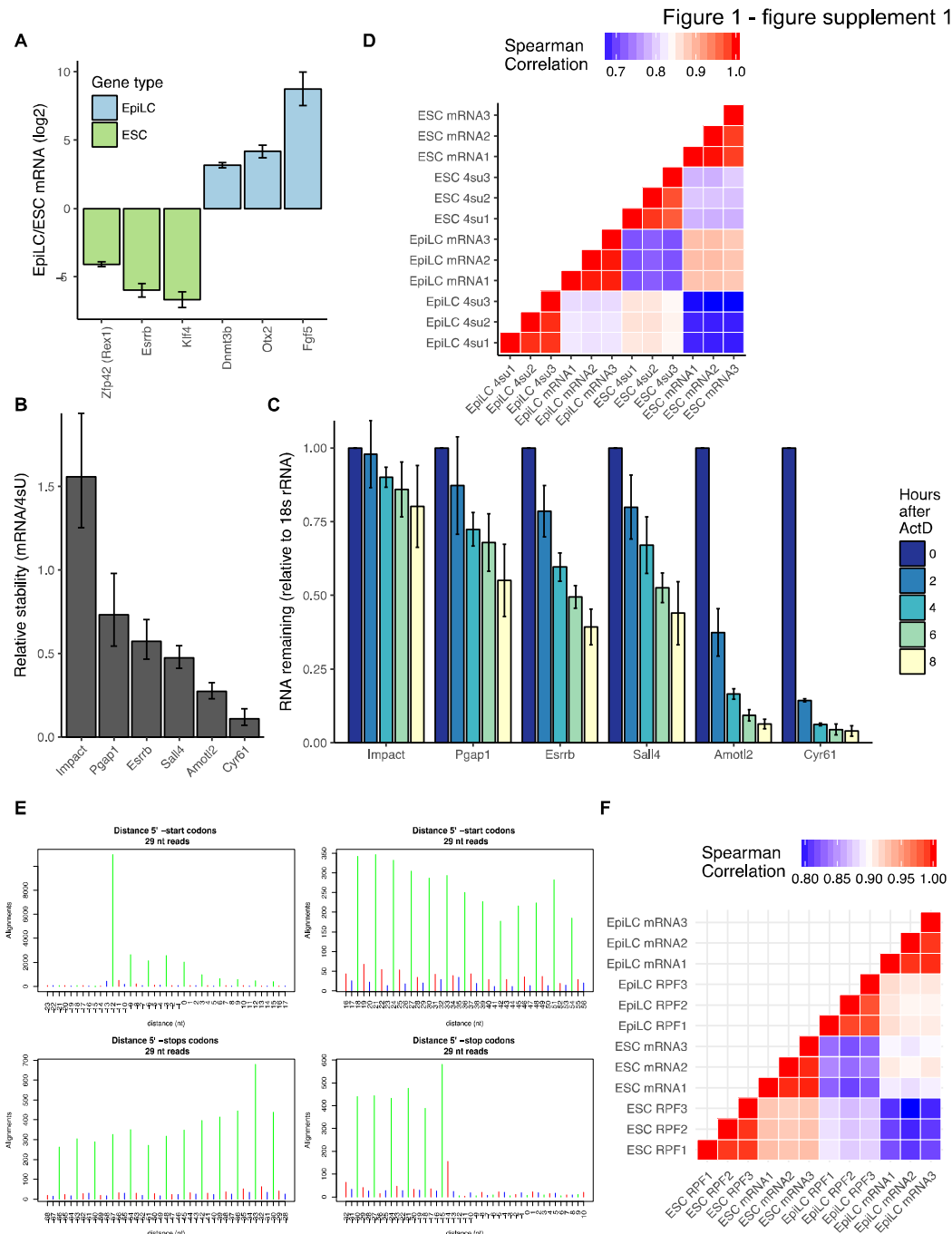
868

869

Figure 1 - figure supplement 1

Figure 1 - figure supplement 1 Validation of differentiation, mRNA stability measurements, and ribosome footprinting.

A) Change in expression of key naive and primed genes during the ESC to EpiLC transition based on RNA-Seq. Error bars represent 95% confidence interval. B) Relative mRNA stability of candidate genes based on ratio of mRNA/4sU. Error bars represent 95% confidence interval. C) Validation of 4sU-Seq measured mRNA stabilities with RT-qPCR time course after blocking transcription with Actinomycin D. Values are normalized to 18S rRNA and their 0 hr timepoint. n = 3 for wild type and n = 6 (3 replicates of each *Ddx6* KO line), error bars are standard deviation. D) Spearman correlation of log2(counts per million) of ESC and EpiLC RNA-Seq and 4sU-Seq replicates. E) Ribosome profiling shows characteristic phasing for ribosome protected footprints. F) Spearman correlation of log2(counts per million) of ESC and EpiLC RNA-Seq and ribosome protected footprint (RPF) replicates.
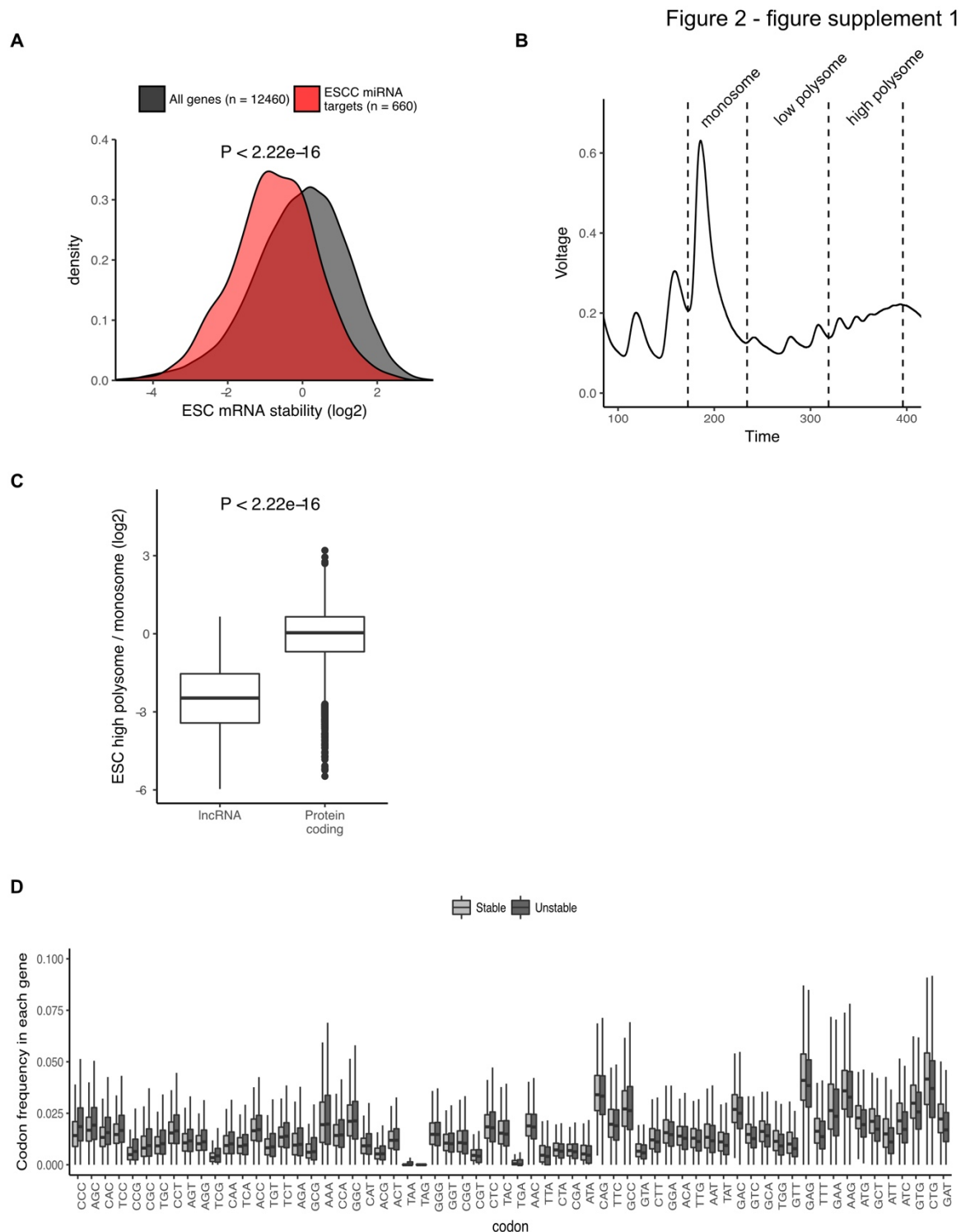
Figure 2 - figure supplement 1 Factors that affect RNA stability in ESCs.
A) mRNA stability of ESCC miRNA targets compared to all mRNAs. P value was calculated using the Mann–Whitney test. B) Polysome trace showing monosome, low polysome, and high polysome fractions collected for RNA-Seq. C) Translation level of long non-coding RNAs (lncRNAs) compared to protein coding RNAs. P value calculated with Mann-Whitney test. D) Boxplots showing the codon usage frequency in the top and bottom 20% of genes in terms of stability. Codons are ordered along the X-axis based on the median codon usage in unstable - median codon usage in stable.

Figure 3 - figure supplement 1

A

891
Figure 3 - figure supplement 1 Characterization of *Ddx6* KO ESCs.
A) Sanger sequencing showing deletion and insertion at the beginning of exon 7 to generate two *Ddx6* KO clones.

895
896
897
898
899
900
901
902
903
904
905
906
907
908
909
910
911
912
913
914
915
916
917
918
919
920
921
922
923
924
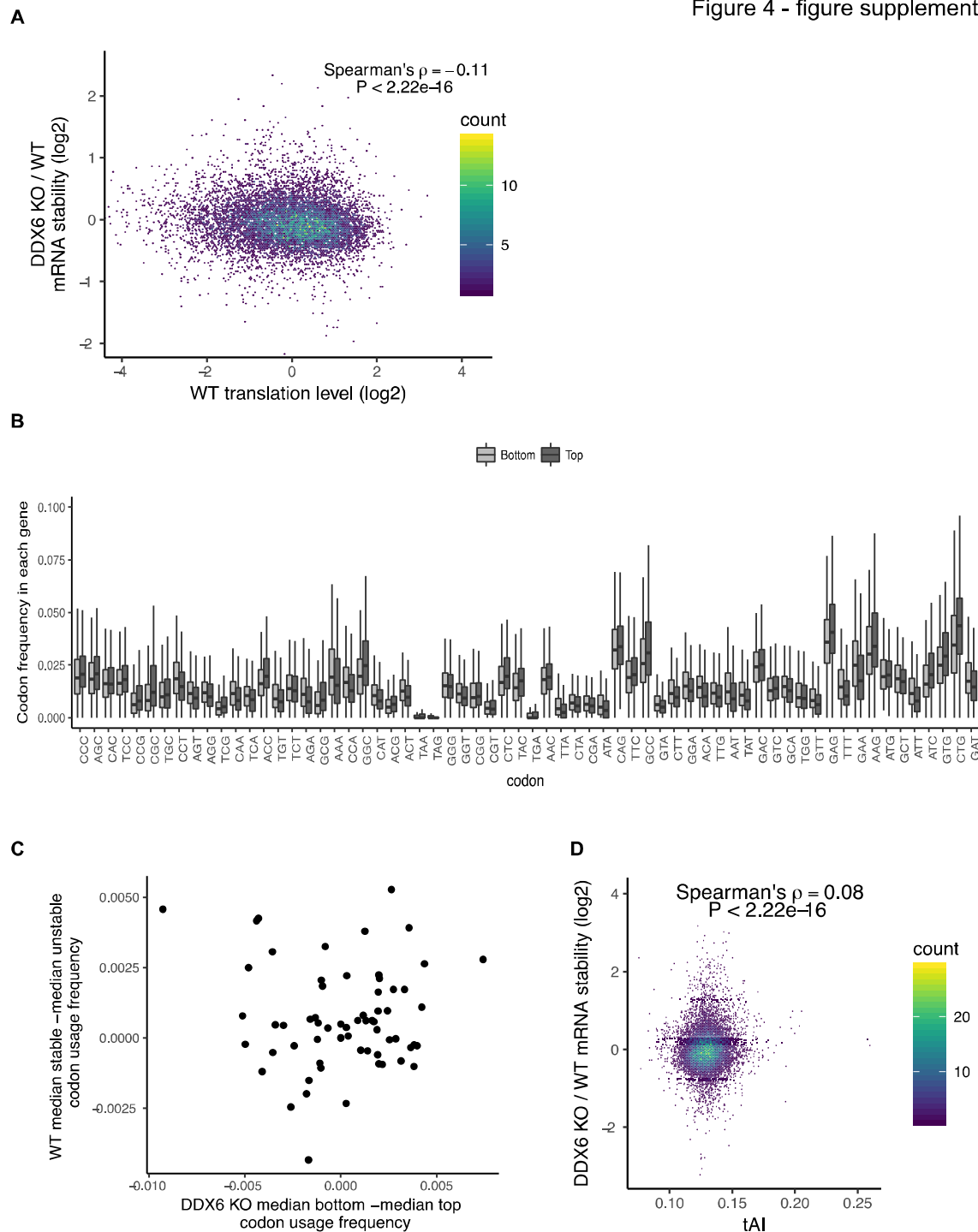925
926
927
928

Figure 4 - figure supplement 1

Figure 4 - figure supplement 1 Connection between stability changes and translation.
A) mRNA stability changes in *Ddx6* KO cells versus wild type translation level. B) Boxplots showing the codon usage frequency in the top and bottom 20% of mRNA stability changes in *Ddx6* KO for unstable genes as defined in Figure S2D. C) Difference in median codon frequency between stable and unstable transcripts in wild type cells versus difference in median codon frequency between top and bottom *Ddx6* KO mRNA stability changes. D) mRNA stability changes in *Ddx6* KO cells versus species specific tRNA adaptation index (tAI) scores for each gene.